J. Phys.: Condens. Matter **23** (2011) 475702 (13pp) doi:10.1088/0953-8984/23/47/475702

Metallurgical phases and their magnetism at the interface of nanoscale MgB_2/Fe layered structures

B Sahoo[1], W Keune[2,3], V Kuncser[4], H-W Becker[5] and R Röhlsberger[1]

[1] Deutsches Elektronen Synchrotron DESY, Notkestraße 85, D-22607 Hamburg, Germany
[2] Fakultät für Physik, Universität Duisburg-Essen, D-47048 Duisburg, Germany
[3] Max-Planck Institut für Mikrostrukturphysik, D-06120 Halle, Germany
[4] National Institute of Materials Physics, 77125, Bucharest-Magurele, Romania
[5] Ruhr-Universität Bochum, Universitätsstraße 150, D-44801, Bochum, Germany

Received 5 August 2011, in final form 10 October 2011
Published 10 November 2011
Online at stacks.iop.org/JPhysCM/23/475702

Abstract

We report on the characterization of metallurgical phases and their magnetism at the interfaces of nanoscale MgB_2/Fe layered structures. MgB_2/^{57}Fe multilayers with varying layer thicknesses were prepared by vacuum deposition and investigated, before and after annealing by electrical resistance measurements, x-ray diffraction and ^{57}Fe conversion-electron Mössbauer spectroscopy (CEMS) down to 5 K. Interfacial Fe–B phases, such as Fe_2B, were identified by CEMS. A superparamagnetic-to-ferromagnetic transition is observed with increasing ^{57}Fe film thickness. Ultrahigh vacuum annealing at 500 °C of the multilayers leads to strong diffusion of Fe atoms into the boundary regions of the MgB_2 layers. MgB_2 in the as-grown multilayers is non-superconducting. Structural disorder and the effect of Fe interdiffusion contribute to the suppression of superconductivity in the MgB_2 films of all the as-grown multilayers and the thinner annealed multilayers. However, an annealed MgB_2/^{57}Fe/MgB_2 trilayer with thicker (500 Å) MgB_2 layers is observed to be superconducting with an onset temperature of 25 K. At 5 K, the annealed trilayer can be conceived as being strongly chemically modulated, consisting of two partially Fe-doped superconducting MgB_2 layers separated by an interdiffused weakly magnetic Fe–B interlayer, which is characterized by a low hyperfine magnetic field B_{hf} of ∼11 T. This chemically modulated layer structure of the trilayer after annealing was verified by Rutherford backscattering.

(Some figures may appear in colour only in the online journal)

1. Introduction

The intermetallic compound magnesium diboride, MgB_2, exhibits a high superconducting transition temperature, T_c, of 39 K in the bulk material [1]. MgB_2 is an intriguing compound both from a fundamental and technological point of view [2]. MgB_2 exhibits a long coherence length (∼5 nm) for the Cooper pairs [3] in contrast to high-T_c cuprate superconductors. For technological purposes, wires and tapes of MgB_2 have been made using the so-called 'powder-in-tube' (PIT) technique [4–9]. Because of their high critical currents, iron-clad superconducting MgB_2 wires are of particular interest [4]. During the consolidation sintering of the MgB_2 core of the wire at high temperatures, the formation of undesirable metallurgical phases at the MgB_2/metal (Fe) interface must be suppressed [4] in order to avoid contamination of MgB_2 grains. Superconducting $Mg_{1-x}Fe_xB_2$ powders have been prepared by mechanical alloying [10]. Furthermore, the rising fundamental interest to study superconductor/ferromagnet proximity effects [11, 12], at and near the superconductor/ferromagnet interface, brings MgB_2/Fe layered structures into focus. Because of these factors there is a significant interest in the metallurgical, chemical and magnetic state on the nanoscale in the interfacial

Table 1. Growth temperature, nominal sample composition, annealing state and superconducting transition temperature T_c (at onset) of the three multilayers.

Sample	Growth temperature (°C)	Sample composition	Thermal treatment	T_c (K)
M1	115	MgB_2 (100 Å)/[^{57}Fe (5 Å)/MgB_2 (100 Å)]$_{15}$/SiO_2/Si(111)	As-prepared	—
			Annealed	—
M2	115	MgB_2 (150 Å)/[^{57}Fe (10 Å)/MgB_2 (150 Å)]$_{10}$/SiO_2/Si(111)	As-prepared	—
			Annealed	—
M3	115	MgB_2 (500 Å)/ ^{57}Fe (40 Å)/MgB_2 (500 Å)/SiO_2/Si(100)	As-prepared	—
			Annealed	25

region of the MgB_2/Fe system. Here, we focus on such a study of the type of metallurgical phases and their magnetism at the MgB_2/Fe interface. Our work presents a first step toward investigation of MgB_2/Fe layered structures with potentially sharp interfaces.

In the present work, we report on the preparation and characterization of the interfacial phases of a MgB_2/^{57}Fe/MgB_2 trilayer and [MgB_2/Fe]$_n$ multilayers. Although there is a vast amount of literature on thin MgB_2 films [2], according to our knowledge this is the first attempt to prepare and investigate MgB_2/Fe multilayers. The topology and the crystallographic structure were characterized by x-ray reflectivity and x-ray diffraction (XRD), respectively. In order to distinguish between different metallurgical phases and magnetic states in a MgB_2/^{57}Fe/MgB_2 trilayer and MgB_2/^{57}Fe multilayers, in the as-prepared and thermally annealed states, ^{57}Fe CEMS was employed. ^{57}Fe CEMS is a powerful technique to probe the local electronic (chemical), metallurgical, magnetic and vibrational properties of ^{57}Fe-containing nanoscale thin films and multilayers and their interfaces on the atomic scale [13–15]. We have employed Rutherford backscattering (RBS) spectroscopy for investigating the layer structure of a thick sample, where low-angle XRD (x-ray reflectivity) is unable to provide information about the layer structure. Furthermore, we studied the conditions for the appearance of superconductivity in the trilayer/multilayers.

2. Preparation and characterization

Three different MgB_2/Fe multilayers (sample codes: M1, M2 and M3) have been grown in a vacuum deposition system (base pressure 2×10^{-9} mbar). MgB_2 layers were grown by co-deposition of the elements [16]. The pressure during co-deposition was 2×10^{-7} mbar. Si(111) or Si(100) wafers with a native oxide layer have been used as substrates. As all substrates are covered by a passive amorphous SiO_2 layer, the choice of the surface orientation of the substrate (whether Si(100) or Si(111)) is unimportant. For deposition purposes the substrates were cleaned by acetone followed by propanol and then by heating in ultrahigh vacuum (UHV) at $\sim 2 \times 10^{-9}$ mbar up to 600 °C for ∼20 min. Evaporation of Mg was performed from a home-made Knudsen cell (alumina crucible). B was evaporated by electron bombardment from a graphite crucible (placed on a water-cooled metal crucible). The purity was 99.98 at.% for Mg and 99.5 at.% for B. At first, deposition rates for Mg and B of 0.38 Å s^{-1} and 0.25 Å s^{-1}, respectively, were chosen. The deposition rates and the thickness of the layers were controlled and measured by calibrated quartz-crystal oscillators. However, because of the high vapor pressure of Mg at high substrate temperatures the magnesium deposition rate had to be deliberately taken slightly higher (0.40 Å s^{-1}) to obtain the required stoichiometry. Aiming at crystallographically textured film growth and considering the low sticking coefficient of Mg at higher temperatures and with the intention to minimize interdiffusion between Fe and MgB_2 layers, the substrate temperature, T_s, during deposition was kept at a convenient value of 115 °C. Evaporation of ^{57}Fe (95% isotopically enriched) was carried out from a Knudsen cell at a rate of 0.1 Å s^{-1}. The nominal geometrical structures of the multilayers are given in table 1. The number of MgB_2/Fe bilayers of M1 and M2 is 15 and 10, respectively. Multilayer M3 is a trilayer (MgB_2/Fe/MgB_2). The multilayers were characterized by XRD, RBS and CEMS.

The multilayer superstructure of samples M1 and M2 has been checked by low-angle XRD (reflectivity) (figure 1). The low-angle XRD pattern of the as-grown multilayer M1 (figure 1(a)) shows dominant peaks with periodic oscillations up to order $n = 5$, indicating good multilayer quality. However, weaker periodic peaks with shorter angular periodicity are present between the labeled ones. We could simulate curve (a) in figure 1, providing satisfying agreement between the simulated (red curve) and experimental (black dots) data. In the simulation we had to assume the existence of two different superstructure periodicities with different weights in as-grown sample M1: (i) one dominant superstructure with shorter spatial periodicity and an intensity contribution of 80%, and (ii) a weaker minority superstructure with a longer spatial periodicity and with an intensity contribution of 20%. The linear superposition of the two types of reflectivity results in the total reflectivity (red curve) in figure 1(a). The average individual layer thicknesses of the MgB_2 layers (t_{MgB_2}) and the Fe layers (t_{Fe}) obtained from the simulation are: $t_{MgB_2} = 75$ Å and $t_{Fe} = 4$ Å, i.e., a periodicity of ∼80 Å (as compared to nominally 105 Å) for the dominant superstructure (i); and $t_{MgB_2} = 225$ Å and $t_{Fe} = 4$ Å, i.e., a periodicity of ∼230 Å for the minority superstructure (ii). In the simulation we assumed increasing interface roughness with growing multilayer thickness. We found that the MgB_2 interface roughness starts from 5 Å for the bottom layer (near the substrate) and increases linearly to 40 Å for the 15th MgB_2 (top) layer. Our results demonstrate that considerable topological roughness evolves for the MgB_2

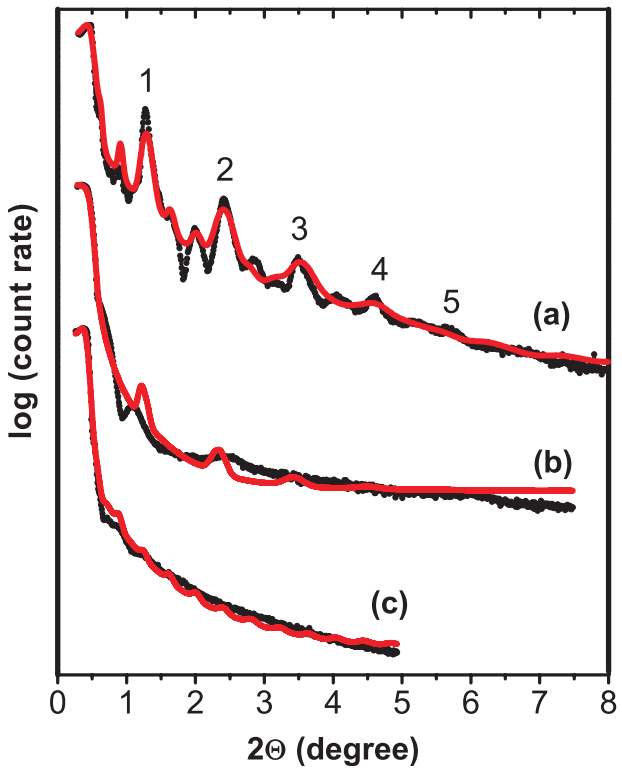

Figure 1. Low-angle XRD pattern of MgB_2/Fe multilayers: sample M1 as-prepared (a) and after annealing (b), and as-prepared multilayer M2 (c). The measured data are shown as black points and the calculated reflectivities are shown as smooth red curves. (Cu Kα radiation).

layer during growth, very likely due to kinetic roughening at our relatively low deposition temperature T_s of only ∼115 °C. The two multilayer periodicities revealed in figure 1(a) (with 80% and 20% intensity contribution, respectively) very likely arise from the larger interface roughness of the MgB_2 layers combined with the discontinuous Fe film growth on MgB_2. This leads to shorter multilayer periodicity (∼80 Å) at such interface regions where neighboring MgB_2 layers are locally separated by Fe islands (clusters), whereas the larger multilayer periodicity (∼230 Å) can originate from lateral interface regions where no Fe clusters are present and neighboring MgB_2 layers are interconnected. Evidently, as-grown sample M1 consists of Fe clusters which are embedded and laterally as well as vertically distributed between rough MgB_2 layers.

The low-angle XRD pattern of the as-grown multilayer M2 did not show pronounced oscillations (figure 1(c)). This indicates that the multilayer structure is less developed in M2. The average individual layer thicknesses obtained from the simulation (red curve in figure 1(c)) are $t_{MgB_2} = 182$ Å and $t_{Fe} = 8$ Å, with an average bilayer period (∼190 Å). The bilayer thickness extracted from the simulation is close to the nominal bilayer period of 165 Å. The MgB_2 interface roughness is similar to that of multilayer M1, i.e., the roughness starts from 5 Å for the bottom layer (near the substrate) and increases linearly to 38 Å for the tenth MgB_2 (top) layer. For multilayer M3 (trilayer) the larger thickness (and probably larger roughness) of the individual and total layers prevents the observation of intensity oscillations by low-angle XRD (not shown).

Annealing the multilayers at 500 °C for 2.5 h in ultrahigh vacuum (UHV) (2×10^{-9} mbar) causes atomic interdiffusion between the ^{57}Fe and MgB_2 layers across the interface, leading to chemically modulated multilayer structures. This is proven by the low-angle XRD pattern of the annealed multilayer M1 (figure 1(b)), where the intensity of the superstructure peaks is heavily reduced after annealing. The average individual layer thicknesses obtained from the simulation (red curve in figure 1(b)) are $t_{MgB_2} = 70$ Å and $t_{Fe} = 2$ Å, with an average bilayer period (∼72 Å). This suggests that the bilayer period of the dominant superstructure is roughly retained after annealing the multilayer. The minority superstructure is not detectable any more after annealing M1. The MgB_2 interface roughnesses obtained from the calculated curve shows that the roughness starts from 30 Å for the bottom layer (near the substrate) and increases linearly to 60 Å for the 15th MgB_2 (top) layer.

Concerning the high-angle XRD results on multilayer samples M1, M2 and M3, no Bragg peak of MgB_2 has been observed in the as-prepared state. Evidently, the small film thickness and the structural disorder in the as-prepared MgB_2 layers do not result in measurable Bragg reflections. However, after annealing the multilayers at 500 °C for 2.5 h in UHV, the MgB_2(002) Bragg peak near 52° clearly appears for multilayer M1, although it is very broad (figure 2(a)), and evolves weakly for the trilayer M3 (figure 2(c)), but surprisingly is absent for multilayer M2 (figure 2(b)) (see also inset in figure 2).

To demonstrate that the Fe layer is interdiffused but still retains a residue of the layered structure in sample M3 (trilayer) after annealing, a Rutherford backscattering measurement was performed using a singly charged He beam with a beam current of 35 nA at the Dynamitron accelerator in Bochum. The beam is collimated to a beam spot of 1 mm diameter on the sample. The backscattered particles are measured with a silicon detector under an angle of 160° with respect to the beam axis in Cornell geometry. The solid angle of the detector and the beam integration have been determined with a radioactive source and a calibrated current source as well as with standard samples and are known with an accuracy of 3%. The data were analyzed with the program RBX [17].

The relevant part of the spectrum is shown in figure 3(a). At backscattering energies between 1350 and 1550 keV the signal from the iron is clearly to be seen. At lower energies one can identify signals from Mg, O, C and B, with high energy edges at about 1050 keV, 752 keV, 530 keV and 460 keV, respectively, all of which are superimposed by the signals from the silicon substrate. The strong contaminant of oxygen and the smaller amount of carbon can unsurprisingly be explained by the preparation procedure as well as by the aging and storage conditions (in air at room temperature for a period of some years) of the annealed sample M3.

As can be easily seen by the shape of the Fe signal the annealed sample M3 is not homogeneous in depth but shows a layer structure. For a sufficient simulation of the data (red line in figure 3(a)) one has to assume at least three layers with

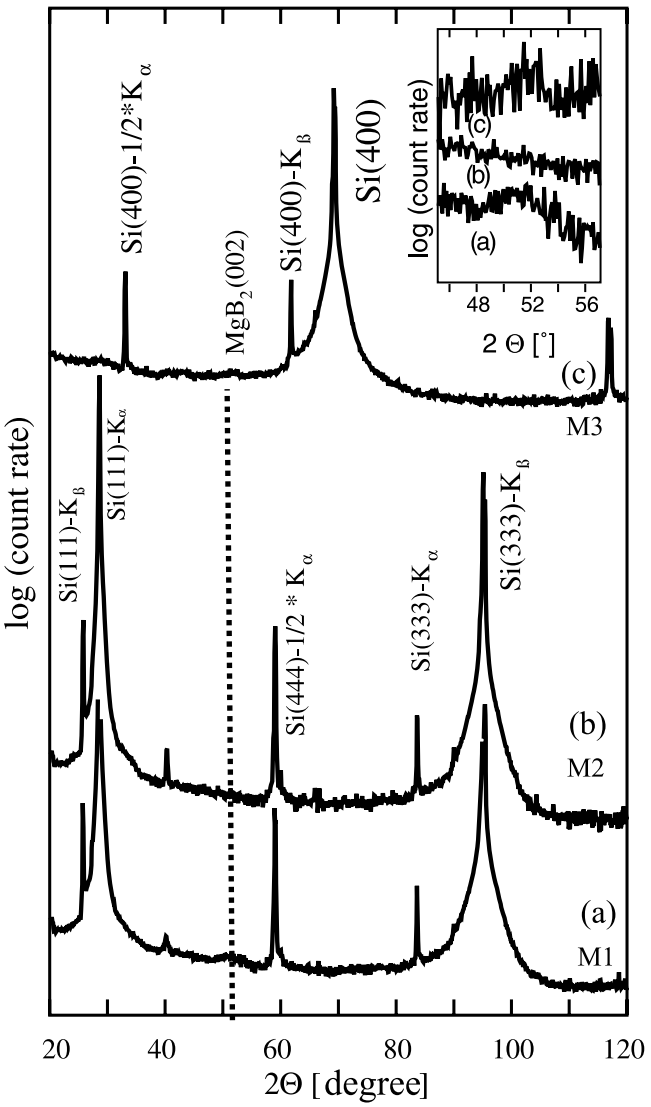

Figure 2. XRD pattern of MgB_2/Fe multilayers M1 (a), M2 (b) and M3 (c), after annealing in UHV at 500 °C for 2.5 h. The dotted line indicates the position of the MgB_2(002) Bragg peak. The peak near 40° in (b) and (c) is of unknown origin. Inset: zoom of the region near $2\Theta = 52°$. (Cu Kα radiation).

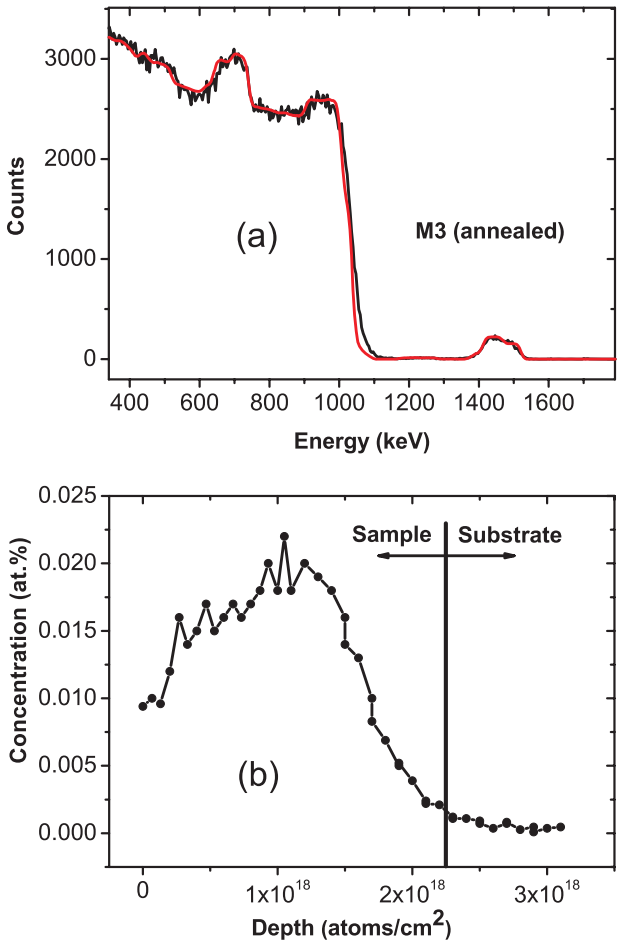

Figure 3. (a) Measured (black line) and simulated (red smooth curve) Rutherford backscattering spectrum for the sample M3 (trilayer) after annealing at 500 °C for 2.5 h in UHV. (b) Depth profile of Fe deduced from the Fe peak shape between 1350 and 1550 keV in (a). The depth of the substrate and sample interface as determined from the shift of the silicon edge in (a) is indicated.

varying relative concentrations of the different elements. The ratio between Mg and B however has been fixed to 1:2; so one can conclude that the RBS analysis is not in contradiction with the assumption of this stoichiometry. It should be noted that the discrete three layers have been assumed for an easy simulation only; the relative concentrations vary most probably continuously as can be expected from diffusion during the annealing of the sample.

This can be seen clearly if the signal of the Fe, which is background free and not interfering with signals from other elements, is converted into a depth profile, as shown in figure 3(b). The depth of the interface between the layer and the substrate which can be accurately determined from the energy shift of the silicon edge relative to the surface value is indicated in the figure. The concentration of the Fe has a maximum in the center of the layer and decreases to the surface as well as (to a stronger extent) to the interface with Si. It is obvious that the original narrow (as-prepared) iron layer has diffused into the MgB_2 layers. The diffusion toward the surface is somewhat stronger, indicating that the two MgB_2 layers might have different chemical or structural properties.

From the integral of the iron peak one can determine the areal density of the iron atoms to be $(3.18 \pm 0.15) \times 10^{16}$ atoms cm^{-2}. This is in very good agreement with the areal density of a 4 nm layer of iron of 3.39×10^{16} atoms cm^{-2} (the nominal value from the preparation) when the bulk density of iron is assumed. Thus no significant amount of iron was lost since the sample preparation.

^{57}Fe CEMS has been used for the study of magnetism and for the detection and characterization of metallurgical phases in the three MgB_2/^{57}Fe multilayer samples. A ^{57}Co (Rh matrix) Mössbauer source of ∼100 mCi activity was employed. For the RT-CEMS measurements a (high-purity He + 4% CH_4) gas-flow proportional counter was used. Low-temperature CEMS measurements were performed at 5 K by using a channeltron detector located (together with the sample) inside the evacuated central tube of a variable-temperature liquid-helium bath cryostat. The spectra were

least-squares fitted using the NORMOS computer program written by Brand [18]. Following the literature, all isomer shift (δ) values are given with respect to a standard bulk α-Fe absorber at room temperature. For the conversion of the measured isomer shifts (using the ^{57}Co(Rh) source) to isomer shifts relative to the α-Fe standard, the following relation was used: $\delta = +0.106$ mm s^{-1}(calibrated) + δ(measured), where δ (measured) can be positive or negative. The electrical resistance measurements were performed by the standard four-point probe method. Both the as-prepared and thermally annealed multilayers were analyzed.

3. Magnetism and metallurgical phase analysis

Phase analysis by Mössbauer spectroscopy is based on the similarity of the observed ^{57}Fe hyperfine parameters of the samples (hyperfine magnetic field, $B_{\rm hf}$, isomer shift, δ, quadrupole splitting, QS, and quadrupole nuclear level shift, ε) with the known parameters of bulk Fe–B phases. The possible phases that form in an MgB_2–Fe powder system after solid state reaction were reported earlier [19, 20]. According to these references, crystalline secondary phases of ferromagnetic Fe_2B and FeB can form, and, moreover, Fe atoms can diffuse into the MgB_2 phase. Here, the Fe atoms are thought to substitute Mg atoms in the MgB_2 lattice due to their smaller mismatch in atomic radii (1.50 Å for Mg, 1.40 Å for Fe and 0.80 Å for B) [21]. Bulk crystalline (c-)FeB, c-Fe_2B [22–24] and c-Fe_3B [25] as well as bulk amorphous (a-)Fe–B [26–28] phases have been thoroughly investigated by Mössbauer spectroscopy. One observes a well resolved Zeeman sextet with $B_{\rm hf} \sim 12$ T and ~13 T for c-FeB at RT and 4.2 K, respectively, and with $B_{\rm hf} \sim 24$ T and ~25 T for c-Fe_2B at RT and 4.2 K, respectively. For a-FeB the hyperfine field has a broad probability distribution, depending on the Fe environment, averaged at $\langle B_{\rm hf}\rangle \sim 16$ T at 4.2 K, while for the distribution of a-Fe_2B the average field $\langle B_{\rm hf}\rangle$ is ~23 T at 4.2 K [26, 27]. c-Fe_3B has three Fe lattice sites with hyperfine fields $B_{\rm hf}$ of about 24, 28 and 30 T at 4.2 K [25]. For comparison, a-Fe_3B exhibits $\langle B_{\rm hf}\rangle \sim 25$ T at RT and 29 T at 4.2 K [25]. Superparamagnetic particles of Fe–B catalysts (assigned to FeB and/or Fe_2B) also have been investigated by Mössbauer spectroscopy [29]. At RT, these iron boride particles exhibit quadrupole-split doublets in the Mössbauer spectra, with a range of quadrupole splittings $\Delta = {\rm QS} = e^2qQ/2$ of 0.62–0.65 mm s^{-1} and isomer shifts δ of 0.22–0.24 mm s^{-1} (relative to α-Fe at RT), while $\Delta = {\rm QS} = 0.67$ mm s^{-1} and $\delta = 0.24$ mm s^{-1} at 77 K. It should be noticed that the Mössbauer parameters of superparamagnetic Fe–B nanoparticles (very likely of the c-FeB phase) [29] and a certain substitutional Fe impurity site in the MgB_2 lattice (doublet D1 in [20]) apparently and accidentally are very similar. On the other hand, the non-mixing nature of Mg and Fe [21] prevents Fe–Mg alloying or compound formation. We used the known hyperfine parameters of bulk Fe–B phases as a fingerprint to identify the Fe–B phases that are possibly formed in our MgB_2/^{57}Fe multilayers.

Room-temperature (RT = 295 K) and low-temperature ($T = 5$ K) CEM spectra of the three as-prepared multilayers M1, M2 and M3 are shown in figures 4 and 5, respectively. At both temperatures, a continuous transition from a non-magnetic to a magnetically ordered state is observed as one goes from the lower to the higher individual Fe layer thickness, $t_{\rm Fe}$, in the multilayers. A non-magnetic/magnetic transition with increasing $t_{\rm Fe}$ is also observed in the RT and low-temperature (5 K) CEM spectra of the multilayers M1, M2 and M3 after annealing at 500 °C for 2.5 h in UHV (figures 6 and 7, respectively).

3.1. As-prepared samples

The CEM spectra of the as-prepared samples are discussed first. The as-prepared multilayer M1 (with the smallest ^{57}Fe thickness of $t_{\rm Fe} = 5$ Å) gives rise to an electric quadrupole-split doublet at RT (figure 4(a)). A quadrupole doublet proves the existence of ^{57}Fe atoms in a non-cubic atomic environment and in a non-magnetic or superparamagnetic state. This doublet (and all other doublets measured here, see below) is found to be asymmetric with respect to line intensities and linewidths, i.e., the left doublet line has systematically lower intensity and larger linewidth than the right line. This is a typical feature of a distribution of quadrupole splittings, QS, correlated with a distribution of isomer shifts, δ, which is often encountered in non-magnetic structurally and/or chemically disordered Fe alloy systems. Therefore, all spectral doublet components measured here were least-squares fitted with a distribution of quadrupole splittings, P(QS), linearly correlated with the isomer shift δ. For sample M1, the distribution P(QS) and the Mössbauer parameters obtained from the fitting are given in figure 4(a) (right-hand side) and in table 2, respectively. At RT, the as-prepared sample M1 exhibits an average quadrupole splitting, $\langle$QS$\rangle$, of 0.68 mm s^{-1}and a peak in the distribution at QS = 0.60 mm s^{-1}. Its small positive average isomer shift of $\langle\delta\rangle = 0.185$ mm s^{-1} indicates the metallic state of the Fe atoms and excludes the presence of Fe-oxides. For sample M1 at 5 K, this doublet partially transforms to an additional broad pattern fitted as a broad singlet (figure 5(a)). Considering the rough surface and the island structure of the single layer MgB_2 films determined earlier by atomic force microscopy [16], and considering the low ^{57}Fe coverage of only 5 Å, one can expect the growth of nanoscale islands of Fe_xB_{1-x} with a wide particle size distribution. These Fe–B nanoclusters behave superparamagnetically at RT, showing the observed doublet. The blocking temperature of the small Fe–B nanoparticles is near 5 K, and the relatively reduced magnetic relaxation rate of the largest nanoclusters in the size distribution gives rise to a relaxed magnetic pattern taken into account by the additional broad singlet at 5 K, figure 5(a). As indicated by the small positive isomer shift and significant quadrupole splitting, the clusters do not consist of pure Fe, but have partially reacted (at least at their interface) with B atoms of the MgB_2 films, forming the above mentioned superparamagnetic Fe–B phase. A small fraction of the deposited ^{57}Fe atoms very likely diffused (at an atomic level) into the MgB_2 layers during deposition [19, 20], forming a paramagnetic state at both RT and 5 K, contributing strongly to the corresponding doublets.

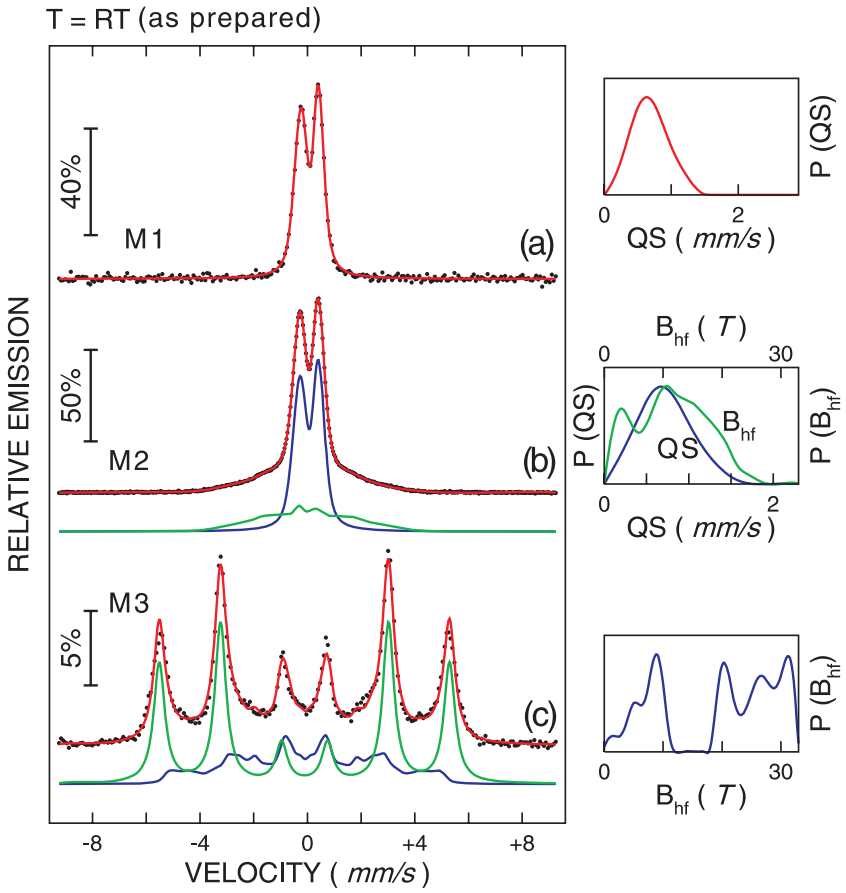

Figure 4. RT-CEM spectra of as-prepared MgB_2/Fe multilayers M1 (a), M2 (b) and M3 (c). The spectra have been least-squares fitted with a distribution of quadrupole splittings P(QS) for multilayer M1, a dominant distribution of quadrupole splittings P(QS) plus a weak distribution of hyperfine magnetic fields $P(B_{hf})$ for multilayer M2, and a Zeeman sextet with sharp lines plus a component with a distribution of hyperfine magnetic fields $P(B_{hf})$ for trilayer M3. The distributions P(QS) and $P(B_{hf})$ are shown on the right-hand side.

However, as the intensity oscillations up to fifth order in the small-angle XRD pattern (figure 1(a)) prove, the multilayer structure is well developed, the $MgB_2/^{57}Fe$ interfaces are fairly sharp, and diffusion is not severe in the as-prepared sample M1, and presumably also in the other as-prepared samples M2 and M3. Reaction of Fe with Mg atoms can be excluded considering the non-mixing nature of Fe and Mg [21].

The Fe-based nanoparticles in the as-prepared second multilayer M2 (with $t_{Fe} = 10$ Å) must have a larger average size (with an Fe-rich core) than those of the multilayer M1 (with $t_{Fe} = 5$ Å). The majority of these larger-sized particles of multilayer M2 are still superparamagnetic at RT, as is evidenced by the quadrupole doublet in figure 4(b). However, an additional broad spectral component of weak relative intensity had to be considered in the fitting. This broad component indicates the evolution of magnetic order and arises from a fraction of larger particles in the size distribution which have a sufficiently slow superparamagnetic relaxation rate even at RT, so that their intrinsic magnetic order becomes observable in the Mössbauer spectrum as the broad magnetic component. This demonstrates that the superparamagnetic blocking temperature of the nanoparticles in M2 is higher than the blocking temperature in M1. This is also confirmed by the CEMS spectrum of M2 (as prepared) at 5 K (figure 5(b)) via the appearance of the broad magnetic component with considerable relative intensity (figure 5(b)). This broad component is attributed to those (larger) Fe–B nanoparticles in M2 whose superparamagnetic relaxation rate is drastically slowed down or maybe even blocked at 5 K, revealing the magnetically ordered state with a large magnetic hyperfine splitting. The spectra in figures 4(b) and 5(b) were fitted with a distribution P(QS) of quadrupole splittings (as described above for sample M1) plus a distribution $P(B_{hf})$ of hyperfine magnetic fields, B_{hf}, in order to take care of the broad additional spectral component. In the fitting of the $P(B_{hf})$ distribution, the hyperfine field B_{hf} was linearly correlated with the isomer shift δ [25]. Further, an effective quadrupole nuclear level shift ε and an in-plane Fe spin direction was considered in the fitting of $P(B_{hf})$, the latter because of the expected magnetic shape anisotropy of the magnetically ordered state. The obtained distributions P(QS) and $P(B_{hf})$ are displayed in figures 4(b) and 5(b) (right-hand side). The Mössbauer parameters obtained from the fittings are given in table 2.

At RT, the doublet distributions P(QS) and the corresponding Mössbauer parameters of samples M2 and M1 (both as prepared) are rather similar, and the same is

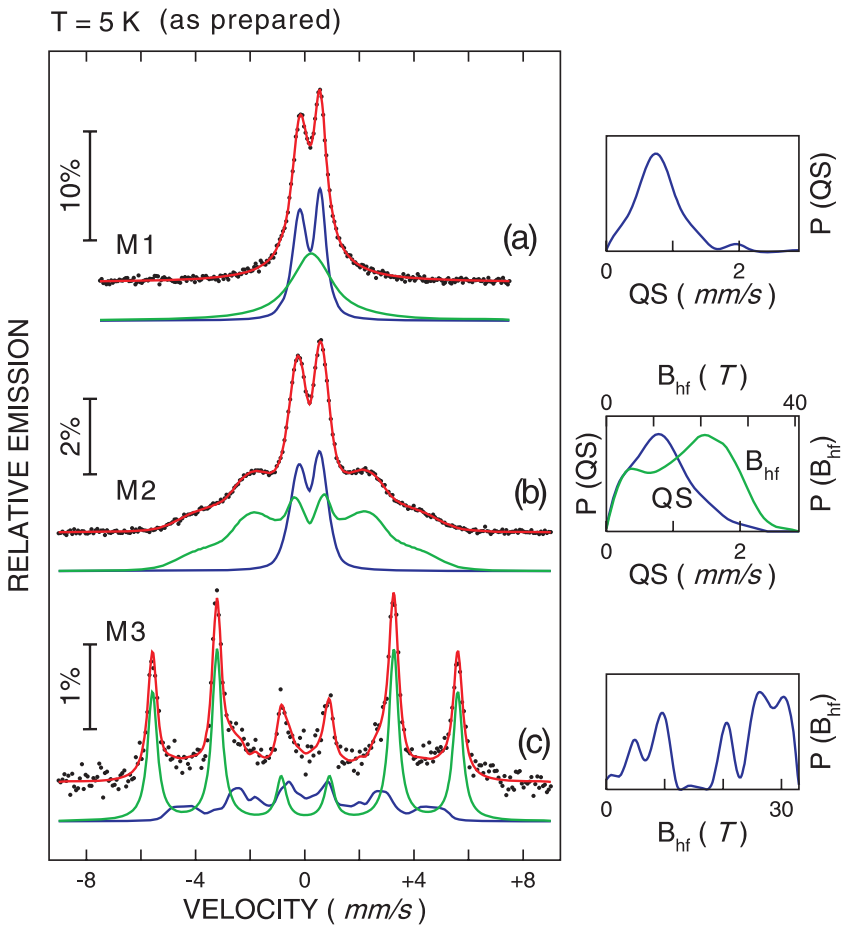

Figure 5. Low-temperature CEM spectra, taken at 5 K, of as-prepared MgB_2/Fe multilayers M1 (a), M2 (b) and M3 (c). The spectra have been least-squares fitted with a distribution of quadrupole splittings P(QS) plus a broad single line for multilayer M1, a distribution of quadrupole splittings P(QS) plus a distribution of hyperfine magnetic fields $P(B_{hf})$ for multilayer M2, and a Zeeman sextet with sharp lines plus a distribution of hyperfine magnetic fields $P(B_{hf})$ for trilayer M3. The distributions P(QS) and $P(B_{hf})$ are shown on the right-hand side.

valid for their parameters at 5 K. This demonstrates that the ^{57}Fe atoms that create these doublets essentially form the same non-magnetic or superparamagnetic metallurgical phase in both samples. As mentioned above, one cannot rule out the formation of some Fe–B phase at the interface of the Fe particles due to the film deposition process and the high chemical reactivity of Fe and B atoms, and also slight diffusion of ^{57}Fe atoms into the MgB_2 films. For the doublets of the as-prepared samples at RT, the average isomer shift $\langle\delta\rangle$ is 0.185 mm s^{-1} and the average quadrupole splitting $\langle$QS$\rangle$ is 0.68 mm s^{-1} for sample M1, while $\langle\delta\rangle = 0.168$ mm s^{-1} and $\langle$QS$\rangle = 0.73$ mm s^{-1} for M2. If we compare these values with the corresponding RT-Mössbauer parameters of crystalline and amorphous Fe–B phases published in the literature, we come to the conclusion that the RT parameters of the doublet distributions of the as-prepared samples M1 and M2 fit closest to the RT-Mössbauer parameters of superparamagnetic particles of c-FeB and/or c-Fe_2B, namely $\delta = 0.22$–0.24 mm s^{-1} and QS = 0.62–0.64 mm s^{-1} [29]. Most likely our doublets originate from the c-Fe_2B phase which exhibits $\delta = 0.17$ mm s^{-1} at RT [30], in good agreement with our $\langle\delta\rangle$ values. This conclusion is supported also by our low-temperature (5 K) isomer-shift values measured on M1 and M2 (both as prepared), namely $\langle\delta\rangle = 0.292$ mm s^{-1} for M1 and $\langle\delta\rangle = 0.271$ mm s^{-1} for M2, which compare reasonably well with the published isomer shift of bulk c-Fe_2B of $\delta = 0.23$ mm s^{-1} at 4.2 K (relative to α-Fe at RT) [30]. Since the low-temperature isomer shift of $\delta = 0.39$ mm s^{-1} for c-FeB at 4.2 K [22] is definitely larger than our low-temperature δ values, the c-FeB phase appears to be unlikely in our as-prepared samples M1 and M2. Thus, the most likely Fe–B phase that contributes predominantly to our doublet distributions P(QS) in the as-prepared samples M1 and M2 is superparamagnetic c-Fe_2B. However, the crystallization of such clusters is very poor and a high degree of disorder is expected even in crystalline grains.

The origin of the hyperfine-field distribution $P(B_{hf})$ can be best inferred from the data in figure 5(b) of the as-prepared sample M2 at 5 K, where the spectral component with $P(B_{hf})$ is relatively strong. Here, the average hyperfine magnetic field $\langle B_{hf}\rangle$ is ∼17 T. Moreover, $P(B_{hf})$ shows a main peak at ∼22 T and extends to high B_{hf} values of up to ∼35 T. It is interesting that the most-probable hyperfine field of ∼22 T is close to the B_{hf} value of ∼25 T of bulk c-Fe_2B at 4.2 K [25], as well as to the average B_{hf} value of ∼23 T of a-Fe_2B [26]. This suggests that the dominant part of this $P(B_{hf})$ distribution very likely

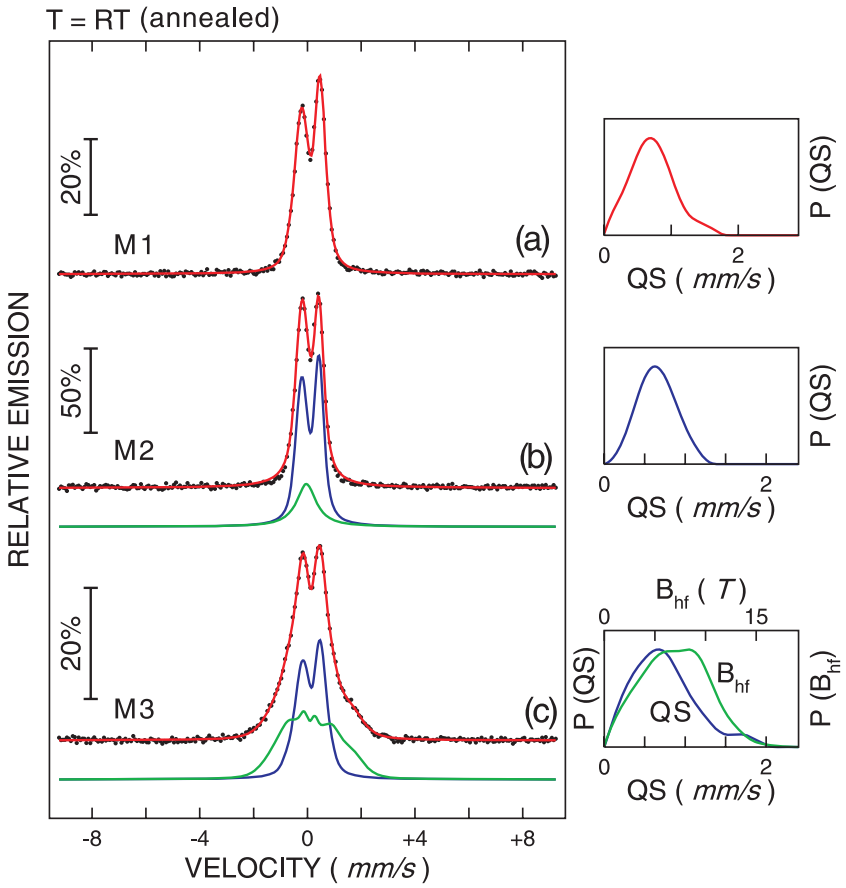

Figure 6. RT-CEM spectra of MgB_2/Fe multilayers M1 (a), M2 (b) and M3 (c), after annealing at 500 °C for 2.5 h in UHV. The spectrum of multilayer M1 was least-squares fitted with a distribution of quadrupole splittings P(QS), the spectrum of M2 with a distribution P(QS) plus a weak singlet, and the spectrum of trilayer M3 with a distribution of quadrupole splittings P(QS) plus a distribution of hyperfine magnetic fields $P(B_{hf})$. The distributions P(QS) and $P(B_{hf})$ are shown on the right-hand side.

originates from structurally disordered Fe_2B nanoparticles, whose magnetic relaxation, however, is not yet completely blocked at 5 K because their hyperfine field of ∼22 T is lower than the low-T value of ∼25 T for bulk c-Fe_2B. The additional contribution to the low-field region of $P(B_{hf})$ might originate from hyperfine fields of a fraction of ^{57}Fe atoms that have diffused into the MgB_2 layers and from hyperfine fields of very small Fe_2B nanoclusters, which show weak magnetic order at 5 K. On the other hand, the extension of $P(B_{hf})$ to such high values as ∼35 T in figure 5(b) provides evidence that bcc Fe also plays a role here, because bulk iron exhibits a hyperfine magnetic field of ∼34 T at 4.2 K. We think that the largest nanoparticles in the as-prepared sample M2 contain a core of chemically unreacted bcc Fe and a surface of c-Fe_2B. However, considering a wide size distribution of the nanoparticles, the most realistic composition may correspond to Fe–B nanoparticles with a defected structure presenting a compositional gradient at Fe-rich cores and B-rich surfaces.

The as-prepared multilayer M3, which in fact is a trilayer with a fairly thick (40 Å) ^{57}Fe layer between two 500 Å thick MgB_2 layers, shows magnetic order both at RT and at 5 K (figures 4(c) and 5(c), respectively). This follows from the observation of Zeeman-split six-line spectra in figures 4(c) and 5(c). Obviously, the 40 Å ^{57}Fe coverage is above the critical film thickness for magnetic percolation of the Fe islands, and a closed film structure has developed, accompanied by the disappearance of superparamagnetism and the appearance of long-range ferromagnetism. Each of the two CEM spectra was least-squares fitted with a dominant Zeeman sextet with relatively sharp lines. Since, however, the measured peaks were observed to be non-Lorentzian and show asymmetric shape, an additional weaker spectral component had to be included in the fitting, described by a distribution of hyperfine magnetic fields, $P(B_{hf})$. B_{hf} in the distribution was assumed to be linearly correlated with the isomer shifts δ. The $P(B_{hf})$ distributions and the Mössbauer parameters obtained from the fittings are shown in figures 4(c), 5(c) and table 2, respectively. The dominant sextet, which has a hyperfine field of $B_{hf} = 33.5$ T at RT and 34.7 T at 5 K, can be unambiguously assigned to the bcc-Fe phase in the Fe layer. The $P(B_{hf})$ distributions in figures 4(c) and 5(c) show a high-field region within ∼18 T $\leq B_{hf} \leq$ ∼33 T and a low-field region within 0 T $\leq B_{hf} \leq$ ∼13 T, separated by a gap between ∼13 and ∼18 T. The local maxima seen in the two field regions indicate preferred local configurations around Fe atoms, suggesting the formation of crystalline Fe–B compounds. It is worth mentioning that the existence of the gap is physically sound, because it always appeared even when different mathematical conditions for the fitting routine

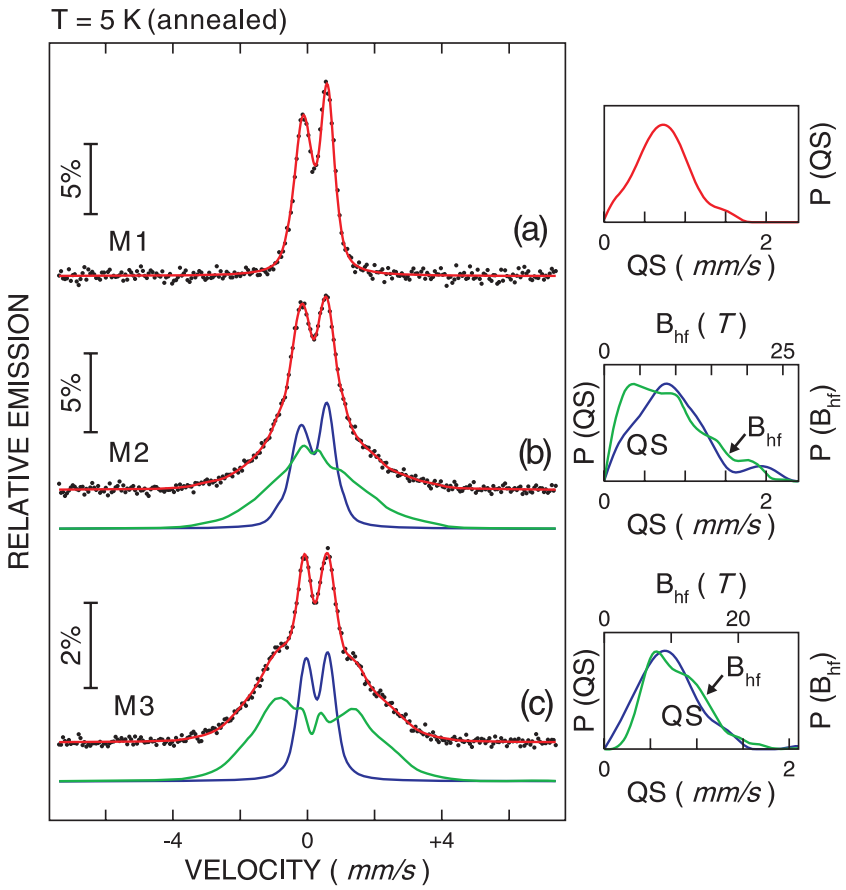

Figure 7. Low-temperature CEM spectra, taken at 5 K, of MgB_2/Fe multilayers M1 (a), M2 (b) and M3 (c), after annealing in UHV at 500 °C for 2.5 h. The spectra were least-squares fitted with a distribution of quadrupole splittings P(QS) for multilayer M1, with a distribution of quadrupole splittings P(QS) plus a distribution of hyperfine magnetic fields $P(B_{hf})$ for multilayer M2, and with a distribution of quadrupole splittings P(QS) plus a distribution of hyperfine magnetic fields $P(B_{hf})$ for trilayer M3. The distributions P(QS) and $P(B_{hf})$ are shown on the right-hand side.

were chosen. Comparison with the literature shows that the high-field region encompasses the hyperfine magnetic fields of bulk c-Fe_2B (∼24 T at RT and ∼25 T at 4.2 K [30]) and of bulk c-Fe_3B (∼24, ∼28 and ∼30 T at 4.2 K [25]). Further, the low-field $P(B_{hf})$ region just includes the hyperfine magnetic fields of bulk c-FeB (∼12 T at RT [24] and ∼13 T at 4.2 K [25]) as limits, and the lower field region may be attributed to Fe_xB_{100-x} amorphous alloys with $x \leq 50$ [26], and, further, to ^{57}Fe atoms diffused into MgB_2 and possibly showing weak magnetic order. Summarizing, there is evidence that the phase composition of the $^{57}Fe/MgB_2$ interfaces in the as-prepared sample M3 is rather complex, and that it is likely that c-Fe_3B, c-Fe_2B, c-FeB and a-Fe_xB_{1-x} phases constitute this interface region.

3.2. Annealed samples

In the following we will discuss the CEM spectra of our three samples M1, M2 and M3 after annealing in UHV at 500 °C for 2.5 h. The spectra taken at RT and 5 K are shown in figures 6 and 7, respectively. Modifications can be observed in the spectra after annealing the samples, as compared to those of the as-prepared samples (shown in figures 4 and 5).

The RT spectrum of the annealed multilayer M1 (figure 6(a)) (with $t_{Fe} = 5$ Å) apparently looks similar to that of the as-prepared sample M1 (figure 4(a)): both spectra show asymmetric quadrupole-split doublets. (All spectral doublet components for the annealed samples were least-squares fitted in the same way as described before for the doublet components from the as-prepared samples.) Also the distribution of quadrupole splittings, P(QS), and the Mössbauer parameters obtained from the fittings (table 2) are similar for the annealed and as-prepared samples M1, although $\langle\delta\rangle$ for M1 (annealed) seems to be slightly larger (by 0.04 mm s^{-1} at RT) than for M1 (as prepared). However, a different behavior of the annealed and the as-prepared M1 samples becomes apparent at 5 K: the quadrupole doublet at RT of the annealed sample retains its shape at 5 K (figure 7(a)), unlike the spectrum of the as-prepared sample M1 (figure 5(a)), for which a broad singlet appeared at 5 K superimposed on the doublet (figure 5(a)). As mentioned in section 3.1, this broad singlet was attributed to a fraction of larger ^{57}Fe–B nanoparticles with a reduced superparamagnetic relaxation rate, and, in addition, to a small fraction of ^{57}Fe atoms that diffused into the MgB_2 matrix during deposition forming small ^{57}Fe clusters and possibly a weakly magnetically ordered state at 5 K. On the other

Table 2. ^{57}Fe hyperfine parameters obtained from the fitting of the Mössbauer spectra of the MgB_2/Fe multilayers. δ = isomer shift in mm s^{-1} (relative to bulk α-Fe at RT), QS = quadrupole splitting in mm s^{-1}, ε = quadrupole nuclear level shift in mm s^{-1}, B_{hf} = magnetic hyperfine field in Tesla, and A = relative spectral area as a percentage. The bracket $\langle\,\rangle$ indicates the average value of the quantity in the brackets. Estimated errors: ±0.01 mm s^{-1} for $\langle\delta\rangle$, ±0.02 mm s^{-1} for $\langle$QS$\rangle$, ±0.4 T for $\langle B_{hf}\rangle$ and B_{hf}, ±0.04 mm s^{-1} for 2ε, and ±5% for A.

Multilayer M1		Multilayer M2		Multilayer M3	
295 K	5 K	295 K	5 K	295 K	5 K
As prepared		As prepared		As prepared	
Doublet distrib. $\langle\delta\rangle = 0.185$ $\langle$QS$\rangle = 0.68$ $A = 100$	Doublet distrib. $\langle\delta\rangle = 0.292$ $\langle$QS$\rangle = 0.81$ $A = 47.4$	B_{hf} distrib. $\langle\delta\rangle = 0.079$ $2\varepsilon = -0.08$ $\langle B_{hf}\rangle = 11.5$ $A = 30.3$	B_{hf} distrib. $\langle\delta\rangle = 0.268$ $2\varepsilon = 0.04$ $\langle B_{hf}\rangle = 17.4$ $A = 70.4$	B_{hf} distrib. $\langle\delta\rangle = 0.017$ $2\varepsilon = -0.04$ $\langle B_{hf}\rangle = 19.4$ $A = 32.9$	B_{hf} distrib. $\langle\delta\rangle = 0.157$ $2\varepsilon = -0.08$ $\langle B_{hf}\rangle = 20.1$ $A = 32.8$
	Singlet $\langle\delta\rangle = 0.351$ $A = 52.6$	Doublet distrib. $\langle\delta\rangle = 0.168$ $\langle$QS$\rangle = 0.73$ $A = 69.7$	Doublet distrib. $\langle\delta\rangle = 0.271$ $\langle$QS$\rangle = 0.85$ $A = 29.6$	Single sextet $\delta = -0.003$ $2\varepsilon = -0.003$ $B_{hf} = 33.5$ $A = 67.1$	Single sextet $\delta = 0.128$ $2\varepsilon = -0.006$ $B_{hf} = 34.7$ $A = 67.2$
Annealed		Annealed		Annealed	
Doublet distrib. $\langle\delta\rangle = 0.227$ $\langle$QS$\rangle = 0.72$ $A = 100$	Doublet distrib. $\langle\delta\rangle = 0.336$ $\langle$QS$\rangle = 0.74$ $A = 100$	Doublet distrib. $\langle\delta\rangle = 0.213$ $\langle$QS$\rangle = 0.65$ $A = 76.8$	B_{hf} distrib. $\langle\delta\rangle = 0.345$ $2\varepsilon = 0.24$ $\langle B_{hf}\rangle = 9.0$ $A = 59.0$	B_{hf} distrib. $\langle\delta\rangle = 0.252$ $2\varepsilon = 0.14$ $\langle B_{hf}\rangle = 7.1$ $A = 51.0$	B_{hf} distrib. $\langle\delta\rangle = 0.319$ $2\varepsilon = 0.19$ $\langle B_{hf}\rangle = 10.7$ $A = 66.2$
		Singlet $\langle\delta\rangle = 0.066$ $A = 23.2$	Doublet distrib. $\langle\delta\rangle = 0.293$ $\langle$QS$\rangle = 0.86$ $A = 41.0$	Doublet distrib. $\langle\delta\rangle = 0.243$ $\langle$QS$\rangle = 0.75$ $A = 49.0$	Doublet distrib. $\langle\delta\rangle = 0.388$ $\langle$QS$\rangle = 0.70$ $A = 33.8$

hand, the smaller (fast relaxing) superparamagnetic Fe–B nanoparticles and the interdiffused isolated paramagnetic ^{57}Fe atoms in the MgB_2 lattice contribute to the doublet even at 5 K. An explanation for the observed spectral modification after annealing is provided by the x-ray reflectivity data shown in figure 1. Here, the annealed sample M1 (figure 1(b)) has lost the pronounced x-ray intensity oscillations of the rather sharp periodic multilayer structure that existed in its as-prepared state (figure 1(a)). This proves the occurrence of severe chemical modulation of the multilayer structure via interfacial interdiffusion due to annealing. Therefore, the observed disappearance of the broad singlet for M1 at 5 K after annealing must be related to the interfacial interdiffusion process. Apparently, during annealing, the fraction of more slowly relaxing larger Fe–B nanoparticles and/or the fraction of magnetically ordered ^{57}Fe clusters in the MgB_2 matrix are dissolved by diffusion, leading to a more extended depth profile of diluted isolated paramagnetic ^{57}Fe atoms in the MgB_2 matrix. The latter state does not exhibit magnetic ordering at 5 K.

Hence, we attribute the observed average isomer shifts of $\langle\delta\rangle = 0.227$ mm s^{-1} at RT and of $\langle\delta\rangle = 0.336$ mm s^{-1} at 5 K for the doublet of the annealed multilayer M1 to Fe–B clusters and to paramagnetic Fe atoms incorporated in the MgB_2 lattice. The small $\langle\delta\rangle$ values indicate the metallic state of these Fe atoms. The corresponding average quadrupole splittings are $\langle$QS$\rangle = 0.72$ mm s^{-1} at RT and $\langle$QS$\rangle = 0.74$ mm s^{-1} at 5 K. ($\langle\delta\rangle$ at RT is smaller than $\langle\delta\rangle$ at 5 K by ∼0.11 mm s^{-1} due to the second-order Doppler shift or thermal red shift.) The Mössbauer parameters of the annealed sample M1 at RT and 5 K and of the as-prepared sample M1 at RT are the most accurate data in table 2, because only one spectral component (the doublet) is involved and small systematic errors due to a superimposed singlet or a magnetic component $P(B_{hf})$ are avoided. Our $\langle\delta\rangle$ and $\langle$QS$\rangle$ values at RT given here are in reasonable agreement with the Mössbauer parameters observed for ^{57}Co-doped MgB_2 at RT, i.e., $\delta = 0.22$ mm s^{-1} and QS = $\Delta = 0.67$ mm s^{-1}(doublet D1 in [20]), which were assigned to ^{57}Co and ^{57}Fe atoms that substitute Mg atoms in the MgB_2 lattice.

The RT-CEM spectrum of the annealed multilayer M2 (figure 6(b)) apparently shows a doublet; however, in order to remain consistent with its asymmetry in line intensities and linewidths, an additional weak broad singlet had to be assumed in the fitting. This weak singlet is a residual of the more apparent $P(B_{hf})$ component for the as-prepared sample M2 at RT (figure 4(b)), which is reduced and modified by ^{57}Fe diffusion during annealing. This is more evident at 5 K, where the relatively strong $P(B_{hf})$ component for M2 (as prepared) in figure 5(b) is reduced in relative intensity (relative spectral area A), and also in the average hyperfine magnetic field $\langle B_{hf}\rangle$ (from ∼17 T (as prepared) to 9 T (annealed), table 2). As described above for sample M1, also for M2 the annealing process results in a relative increase of the doublet intensity due to enhanced ^{57}Fe diffusion into the MgB_2 matrix, connected with an almost complete disappearance of the original Fe–B nanoparticles leading to an extended depth profile of ^{57}Fe atoms in the MgB_2 lattice. The $\langle\delta\rangle$ values for the doublets of the annealed samples M1 and M2 are in good agreement with each other at RT and at

5 K, respectively (table 2). Similarly to M1, the isomer shift of M2 seems to become slightly more positive (by 0.04 mm s^{-1} at RT) due to annealing.

After annealing the MgB_2 (500 Å)/^{57}Fe (40 Å)/MgB_2 (500 Å) trilayer M3, the typical sextet of bcc Fe with its large Zeeman splitting that existed for the as-prepared sample M3 (figures 4(c) and 5(c)) disappears completely, and an asymmetric quadrupole doublet superimposed on a magnetic $P(B_{hf})$ component appears instead (figures 6(c) and 7(c)). The Mössbauer parameters obtained from the least-squares fitting are given in table 2. The corresponding isomer shifts $\langle\delta\rangle$ of the doublets for the annealed samples M1, M2, and M3 are in good agreement with each other, indicating their similar origins. The corresponding $\langle QS\rangle$ values for the different samples after annealing show somewhat larger fluctuations, but they are still in fair agreement with each other. For M3 (annealed) at RT, the relative intensities (relative spectral areas A) of the doublet ($A = 49\%$) and of the $P(B_{hf})$ component ($A = 51\%$) are similar, but at 5 K a considerable amount of doublet intensity (∼15%) has been transformed into the magnetic $P(B_{hf})$ component. This must be related to the larger ^{57}Fe thickness of $t_{Fe} = 40$ Å for M3 as compared to 10 Å (for M2) and 5 Å (for M1). The observed average hyperfine field of $\langle B_{hf}\rangle \sim 11$ T at 5 K is close to the hyperfine field of ∼13 T for bulk c-FeB at low temperature (4.2 K) [25]. This agreement leads us to conclude that a large fraction of the ^{57}Fe atoms in the annealed sample M3 exist in superparamagnetic nanoparticles of the c-FeB phase at RT, contributing partially to the doublet. At 5 K, the superparamagnetic relaxation of these c-FeB nanoparticles is blocked or nearly blocked, leading to the appearance of the $P(B_{hf})$ distribution with $\langle B_{hf}\rangle \sim 11$ T. However, because of the chemical roughening of the MgB_2/Fe interface after annealing (observed by x-ray reflectivity on sample M1), it is reasonable to assume that also for M3 a certain fraction of ^{57}Fe atoms has diffused into the MgB_2 lattice forming isolated Fe atoms or Fe clusters that are paramagnetic at RT and contribute also to the doublet, together with superparamagnetic c-FeB nanoparticles. As mentioned before, one should notice that superparamagnetic Fe–B nanoparticles (very likely of the FeB phase) [29] and Fe atoms incorporated at special sites in the MgB_2 lattice (doublet D1 in [20]) apparently have very similar Mössbauer parameters. We would like to emphasize that the main effect of thermal annealing on all samples is the enhancement of Fe diffusion leading to dissolution of initially larger Fe– and Fe–B clusters. This is observed by a decrease of the magnetic components in the Mössbauer spectra of the annealed samples as compared to the as-prepared samples.

4. Superconductivity

None of the as-prepared MgB_2/^{57}Fe heterostructures were found to be superconducting down to 5 K. Several factors may be responsible for this. As is inferred from the missing MgB_2(002) reflection in the XRD pattern (not shown), the MgB_2 structure is badly developed in these virgin samples, probably due to the very low substrate temperature T_s (∼115 °C) used during deposition [31]. This reduces or

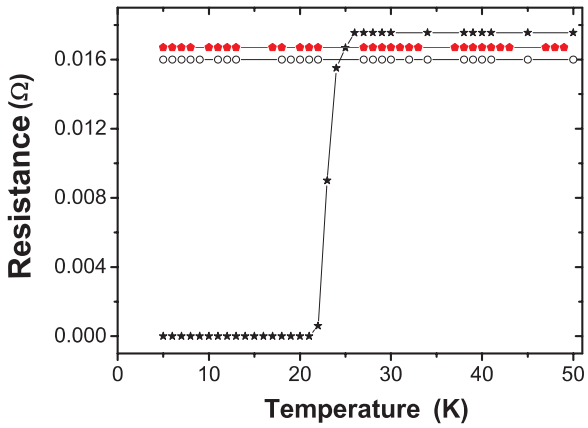

Figure 8. Temperature dependence of electrical resistance of multilayers M1 (empty circles), M2 (filled pentagons), and trilayer M3 (asterisks), after annealing in UHV at 500 °C for 2.5 h. The trilayer M3 becomes superconducting below $T_c \sim 21.5$ K (onset temperature ∼25 K).

suppresses superconductivity. Further, multilayer M1 and M2 contain very thin individual MgB_2 layers (100 Å and 150 Å thick, respectively), and hence the 'size effect' is playing an additional important role in reducing T_c. For multilayer M3 (trilayer) the MgB_2 layers are thicker (500 Å), and a size effect in reducing T_c relative to the bulk value (39 K) is unlikely. Moreover, contrary to samples M1 and M2, the Fe layer in the trilayer M3 is thick enough to show ferromagnetism even at RT, as is demonstrated by the bulk-like hyperfine magnetic field of ∼33 T at RT (figure 4 and table 2). Thus, the ferromagnet/superconductor proximity effect acting at the interfaces may contribute to the suppression of superconductivity in the as-prepared sample M3.

After annealing these samples in UHV at 500 °C for 2.5 h, multilayers M1 and M2 were not found to be superconducting (figure 8), although the crystallographic MgB_2 structure improved for sample M1, as evidenced by the appearance of the MgB_2(002) reflection in the XRD pattern (figure 2(c)). The absence of superconductivity can be due to the small MgB_2 film thickness (size effect) in M1 and M2 and/or to the destructive nature of magnetism on superconductivity. The latter conclusion is based on the observation of magnetic order at 5 K (figure 7(b)) of Fe atoms that diffused into the MgB_2 layers during 500 °C annealing of sample M2. In the case of the annealed sample M1 at $T = 5$ K, magnetic order is not detected by Mössbauer spectroscopy (figure 7(a)); however, the observed quadrupole doublet can be attributed to paramagnetic Fe atoms that diffused into the thin MgB_2 layers with a diffusion length that might be about equal to the MgB_2 film thickness. Then, these paramagnetic Fe magnetic moments might contribute to the collapse of superconductivity.

In contrast to the annealed multilayers M1 and M2, the annealed trilayer M3 with its thicker (500 Å) MgB_2 layers is found to be superconducting, with an onset temperature of 25 K (figure 8), which, however, is smaller than $T_c = 39$ K of the bulk material. Annealing improved the MgB_2

crystallographic order, as is indicated by the appearance of the faint (002) Bragg reflection in figure 2(c), combined with the appearance of superconductivity. As compared to the as-prepared trilayer M3, which is characterized by a ferromagnetic bulk-like bcc-Fe layer with a large hyperfine magnetic field (figure 5(c)) (implying a large magnetic moment that destroys superconductivity), annealing at 500 °C caused the Fe atoms to diffuse into the interfacial regions of the MgB_2 layers, forming either Fe–B clusters or dispersed Fe atoms in the MgB_2 lattice. This resulted in the disappearance of the bcc-Fe layer and in a drastic weakening of magnetism, as observed by the rather small average hyperfine magnetic field of only $\langle B_{hf} \rangle \sim 11$ T at 5 K in the Mössbauer spectrum (figure 7(c) and table 2). One can also assume that the MgB_2 top and bottom layer thickness (500 Å) in M3 is larger than the penetration depth (diffusion length) of the ^{57}Fe atoms and that the ^{57}Fe atoms do not diffuse completely across the MgB_2 film, so that a sufficiently thick region in the MgB_2 layers (away from the original MgB_2/^{57}Fe interface) remains unaffected or only weakly affected by interdiffusion. This unaffected MgB_2 region might be structurally/chemically better ordered than the interdiffused interface region, because the atomic size mismatch between Fe and Mg atoms may induce disorder in the interdiffused zone. It is the unaffected region where superconductivity in sample M3 develops after annealing. The cross-section of the annealed sample M3 thus can consist of interfacial MgB_2 regions, affected by Fe diffusion processes, where weak magnetism prevails, and inner regions which are superconducting. Due to the simultaneous change of the thicknesses influencing T_c, namely t_{MgB_2} and t_{Fe}, the reason for disappearance or appearance of superconductivity in the multilayers or in the trilayer, respectively, could not be identified conclusively. As discussed by Ueda and Naito [31], many experimental parameters influence superconductivity in MgB_2 single layers. For multilayers the situation might become even more complex. A systematic study will be considered in future experiments to investigate the dependence of T_c on t_{MgB_2}, t_{Fe}, substrate temperature T_s, stoichiometry, and other parameters during growth.

5. Summary and conclusions

Nanoscale [MgB_2 (100 Å)/^{57}Fe (5 Å)]$_{15}$ and [MgB_2 (150 Å)/^{57}Fe (10 Å)]$_{10}$ multilayers (samples M1 and M2, respectively) and a MgB_2 (500 Å)/^{57}Fe (40 Å)/MgB_2 (500 Å) trilayer (sample M3) have been prepared by physical vapor deposition of the elements onto oxidized Si substrates. The samples were characterized in their as-grown state and after thermal annealing at 500 °C in UHV by electrical resistance and x-ray diffraction. In addition, the multilayers/trilayer are studied by ^{57}Fe conversion-electron Mössbauer spectroscopy down to 5 K. In the MgB_2/^{57}Fe multilayers, the Fe growth is influenced by the roughness of the underlying MgB_2 layer [16]. As-prepared ultrathin Fe films of 5 and 10 Å in coverage consist of Fe–B nanoparticles embedded between MgB_2 layers, as is evidenced from the superparamagnetic behavior observed via a quadrupole-split doublet by CEMS. By contrast, 40 Å thick ^{57}Fe films (as prepared) are found to be ferromagnetic (as expected for such a large film thickness) with a dominant spectral component from the α-Fe phase. The Mössbauer isomer shift indicates interfacial chemical reaction with boron, and Fe–B phases, such as Fe_2B and FeB, could be identified. In the as-grown state, the MgB_2 films in the multilayers are not superconducting.

Annealing in UHV causes strong interfacial diffusion of ^{57}Fe atoms from the Fe–B nanoparticles into the MgB_2 layers, combined with a decrease of the nanoparticle size. At low temperature (5 K), this leads to the coexistence of a weakly magnetic state in multilayers M2 and M3, characterized by a relatively small average hyperfine magnetic field of ∼9 T and ∼11 T, respectively, and a superparamagnetic and/or non-magnetic state, characterized by the quadrupole doublet. The MgB_2 films in our annealed multilayers with smaller MgB_2 layer thicknesses t of 100 Å (M1) and 150 Å (M2) were found to be too thin to be superconducting at and above 5 K, very likely due to the combined effects of Fe diffusion into the MgB_2 layers and the small MgB_2 layer thickness (size effect). However, the thicker MgB_2 films in the MgB_2 (500 Å)/^{57}Fe (40 Å)/MgB_2 (500 Å) trilayer are observed to be superconducting after annealing, showing an onset temperature of $T_c \sim 25$ K. This demonstrates that superconductivity in the inner ('bulk-like') part of these 500 Å thick MgB_2 layers is not destroyed by the weak magnetism observed in the boundary regions of these layers. Therefore, the annealed MgB_2/Fe/MgB_2 trilayer may be conceived as chemically modulated layers, with two partially Fe-doped 'bulk-like' (central) superconducting MgB_2 layers separated by a low-magnetization (low-hyperfine-field) interdiffused Fe–B interlayer. This chemically modulated proposed layer structure has been verified by RBS spectroscopy.

Acknowledgments

We are grateful to U von Hörsten (Duisburg-Essen) for his excellent technical assistance and J Strempfer (DESY) and Professor M Przybylski (Max-Planck Institute of Microstructure Physics, Halle, Germany) for critically reading the manuscript and for valuable discussions. We are thankful to Oliver Seeck (DESY) for providing the computer program to calculate the x-ray reflectivity curves. Financial support by the Deutsche Forschungsgemeinschaft (GK 277 at Duisburg-Essen) is gratefully acknowledged.

References

[1] Nagamatsu J, Nakagawa N, Muranaka T, Zenitani Y and Akimitsu J 2001 *Nature* **410** 63
[2] for a recent review see Xi X X 2008 *Rep. Prog. Phys.* **71** 116501
[3] Buzea C and Yamashita T 2001 *Supercond. Sci. Technol.* **14** R115
[4] Jin S, Mavoori H, Bower C and van Dover R B 2001 *Nature* **411** 563
[5] Grasso G, Malagoli A, Ferdeghini C, Roncallo S, Braccini V, Siri A S and Cimberle M R 2001 *Appl. Phys. Lett.* **79** 230

[6] Flükiger R, Suo H L, Musolino N, Beneduce C, Toulemonde P and Lezza P 2003 *Physica* C **385** 286
[7] Kováç P, Hušek I, Grovenor Ch and Salter Ch 2003 *Supercond. Sci. Technol.* **16** 1
[8] Braccini V, Nardelli D, Penco R and Grasso G 2007 *Physica* C **456** 209
[9] Kumakura H, Matsumoto A, Nakane T and Kitaguchi H 2007 *Physica* C **456** 196
[10] Gao Y D, Ding J, Chen Q, Rao G V S and Chowdari B V R 2004 *Acta Mater.* **52** 1543
[11] Lazar L, Westerholt K, Zabel H, Tagirov L R, Goryunov Yu V, Garif'yanov N N and Garifullin I A 2000 *Phys. Rev.* B **61** 3711
[12] Gu J Y, You C-Y, Jiang J S, Pearson J, Bazaliy Ya B and Bader S D 2002 *Phys. Rev. Lett.* **89** 267001
[13] Sauer Ch and Zinn W 1993 *Magnetic Multilayers* ed L H Bennett and R E Watson (Singapore: World Scientific)
[14] Przybylski M 1998 *Hyperfine Interact.* **113** 135
[15] Shinjo T and Keune W 1999 *J. Magn. Magn. Mater.* **200** 598
[16] Sahoo B, Kuncser V, Kirsch S and Keune W 2003 *Phase Trans.* **76** 423
[17] Kotay E 1994 *Nucl. Instrum. Methods* B **85** 588
[18] Brand R A 1987 *Nucl. Instrum. Methods* B **28** 398
[19] Kühberger M and Gritzner G 2002 *Physics* C **370** 39
[20] Kuzmann E, Homonnay Z, Klencsár Z, Kühberger M, Vértes A and Gritzner G 2002 *Supercond. Sci. Technol.* **15** 1479
[21] Shinjo T, Kawaguchi K, Yamamoto R, Hosoito N and Takada T 1984 *Chem. Lett.* **13** 59
[22] DeYoung D B and Barnes R G 1975 *J. Chem. Phys.* **62** 1726
[23] Weisman I D, Swartzendruber L J and Bennet L H 1969 *Phys. Rev.* **177** 465
[24] Shinjo T, Itoh F, Takaki H, Nakamura Y and Shikazono N 1964 *J. Phys. Soc. Japan* **19** 1252
[25] Chien C L, Musser D, Gyorgy E M, Sherwood R C, Chen H S, Luborsky F E and Walter J L 1979 *Phys. Rev.* B **20** 283
[26] Chien C L and Unruh K M 1982 *Phys. Rev.* B **25** 5790
[27] Chien C L and Unruh K M 1984 *Phys. Rev.* B **29** 207
[28] Franke H, Dey S, Rosenberg M, Luborsky F E and Walter J L 1980 *J. Magn. Magn. Mater.* **15–18** 1364
[29] Wang C and Bartholomew C H 1990 *Appl. Catal.* **62** 221
[30] Murphy K A and Hershkowitz N 1973 *Phys. Rev.* B **7** 23
[31] Ueda K and Naito M 2003 *J. Appl. Phys.* **93** 2113